Escobar, D.; Ahedo, E. Global stability analysis of azimuthal oscillations in Hall thrusters, *in IEEE Transactions on Plasma Science (Special issue IEPC 2013), 43(1), Nov. 2014, Pp. 149-157*

DOI: https://doi.org/10.1109/TPS.2014.2367913

Global Stability Analysis of Azimuthal Oscillations in Hall Thrusters

Diego Escobar and Eduardo Ahedo

***Abstract*— A linearized time-dependent 2-D (axial and azimuthal) fluid model of the Hall thruster discharge is presented. This model is used to carry out a global stability analysis of the plasma response, as opposed to the more common local stability analyses. Experimental results indicate the existence of low-frequency long-wave-length azimuthal oscillations in the direction of the E × B drift, usually referred to as spokes. The present model predicts the presence of such oscillations for typical Hall thruster conditions with a frequency and a growth rate similar to those found in experiments. Moreover, the comparison between the simulated spoke and the simulated breathing mode, a purely axial low-frequency oscillation typical in Hall thrusters, shows similar features in them. Additionally, the contribution of this azimuthal oscillation to electron conductivity is evaluated tentatively by computing the equivalent anomalous diffusion coefficient from the linear oscillations. The results show a possible contribution to anomalous diffusion in the rear part of the thruster.**

***Index Terms*— Plasma propulsion, plasma simulation, plasma stability, plasma transport processes.**

I. Introduction

HALL effect thrusters (HET) are a type of electric propulsion device whose operation principle is as follows: a radial magnetic field is imposed together with an axial electric field inside a coaxial channel where a neutral gas, typically xenon, is introduced as propellant. Three species of particles are present in a HET: 1) neutrals, which are injected from the rear part of the channel and flow axially toward the thruster exit; 2) electrons, which are introduced by a cathode located just outside the channel and flow upstream toward the anode describing a collisional axial transport together with an azimuthal $\mathbf{E} \times \mathbf{B}$ drift; and 3) ions, which are created from ionization of neutrals due to collisions with the counter-streaming electrons, are unmagnetized, and are accelerated axially by the electric field in the channel and the near plume. The main control parameters of a Hall thruster are the discharge voltage, the magnetic field and the mass flow rate, with the discharge current an output of the dynamical system. For a given magnetic field and mass flow rate, it is possible to represent the evolution of the discharge current as a function of the discharge voltage in the so-called current–voltage (I–V) curve. This curve shows two distinct regimes: 1) a low ionization regime, where the discharge current increases with the voltage and 2) a current saturated regime, where the discharge current is fairly insensitive to changes in the discharge voltage.

Hall thrusters have now become a mature alternative to chemical propulsion in many space applications ranging from orbital raising of satellites through north–south station-keeping of geostationary satellites to low-thrust propulsion of interplanetary probes. However, not all physical processes inside Hall thrusters are fully understood, in particular, the electron perpendicular conductivity. Since the early stages of the Hall thruster technology development, it has been clear that the cross-field electron mobility inside the channel and in the plume is too high to be explained with classical collisionality [1]. That is why the term anomalous diffusion is normally used to refer to the higher than expected electron axial current.

The main properties of the anomalous diffusion, experimentally verified, may be summarized as: 1) it is present in the channel as well as in the plume of the thruster [2], [3]; 2) there is a dip of electron conductivity in the region of high magnetic and electric fields [4], [5]; 3) according to experiments [6], [7], the electron mobility scales as $1/B$ rather than as $1/B^2$, where B is the magnetic field strength; and 4) the magnetic field gradients affect greatly the electron conductivity [8].

Currently, there is no agreement within the Hall thruster community about the mechanism of the anomalous diffusion, but the most accepted explanations are: 1) plasma oscillations, referred to as Bohm-type or turbulent diffusion, based on the fact that correlated azimuthal oscillations of plasma density and electric field would induce a higher electron mobility [9], [10] and 2) near-wall conductivity, where secondary electrons emitted by the walls would cause a net axial current [11]. However, the anomalous diffusion seems to follow a $1/B$ scaling [6], contrary to the $1/B^2$ scaling of the near-wall conductivity. In addition, many simulation codes [12]–[14] that model the near-wall conductivity still need Bohm diffusion to match the electron conductivity measured experimentally. Thus, near-wall conductivity does not seem to explain the anomalous diffusion. On the other hand, several experiments have confirmed with different techniques the presence of azimuthal oscillations. These oscillations are normally grouped in low frequency

Manuscript received November 30, 2013; revised October 16, 2014; accepted November 3, 2014. Date of publication November 20, 2014; date of current version January 6, 2015. This work was supported in part by Spain's Research and Development National Plan under Project AYA-2010-61699 and in part by the Air Force Office of Scientific Research, Air Force Material Command, U.S. Air Force, under Grant FA8655-13-1-3033.

D. Escobar is with the Escuela Técnica Superior de Ingenieros Aeronáuticos, Universidad Politécnica de Madrid, Madrid 28040, Spain (e-mail: descobar@gmv.com).

E. Ahedo is with the Departamento de Bioingeniería e Ingeniería Aeroespacial, Universidad Carlos III de Madrid, Leganés 28911, Spain (e-mail: eduardo.ahedo@uc3m.es).

Color versions of one or more of the figures in this paper are available online at http://ieeexplore.ieee.org.

Digital Object Identifier 10.1109/TPS.2014.2367913

(5–30 kHz), low-to-medium frequency (30–100 kHz), and high frequency (1–10 MHz) oscillations [15]. Some of those experiments show the presence of low-frequency azimuthal oscillations in the rear part of the thruster, in the ionization region [10], [16]–[26]. The analysis of these oscillations, referred to as spokes, is the topic of this paper.

This paper deals with the stability of the Hall discharge from a global point of view, as opposed to the more common local stability analyses. The latter are based on the analysis of the fluid equations at a fixed axial location of the channel and this requires freezing the macroscopic plasma variables and their derivatives, whereas the former method does account consistently for the axial variation of those variables and their linear perturbations. Most of the stability analyses of the Hall discharge in the azimuthal direction carried out so far are local and can be grouped in those that do not account for the ionization process [8], [27]–[31] and those that take it into consideration in the model through particle source terms and fluid equations for the neutral species [17], [32]–[35]. However, all these local stability studies suffer from the problems mentioned above. On the other hand, the few studies that do account globally for the axial variations of the inhomogeneous plasma focus on the high frequency range [36]–[40]. The current study fills the gap of global stability analyses in the low frequency range, where the ionization process plays a very important role.

The rest of this paper is organized as follows. In Section II, the formulation of the linearized time-dependent 2-D model used in this paper is presented. Section III shows and discusses the results from the model, including a comparison against the breathing mode. The possible link between the simulated azimuthal oscillation and the electron cross-field mobility is analyzed in Section IV. Finally, the conclusions are drawn in Section V.

II. Formulation

This section presents the formulation used in this paper. First, the 1-D model of Ahedo *et al.* [41], upon which the 2-D model is based, is summarized. Then, the linearized time-dependent 2-D formulation is presented.

A. 1-D Model

The hypotheses and equations of the 1-D stationary model of Ahedo of the Hall discharge are reviewed in this section. Each one of the species present in a HET (neutrals, electrons, and ions) is accounted for with a separate set of macroscopic fluid equations based on conservation principles of mass, momentum, and energy. Only single-charge ions are considered as multiply charged ions are neglected. Quasi-neutrality is assumed as the Debye length in Hall thrusters is much smaller than the dimensions of the channel. Furthermore, whereas electrons are highly magnetized, ions are considered to be unmagnetized. On the other hand, due to the very low mass of the electrons, electron-inertia terms are neglected in the electron momentum and energy equations. At the same time, ions and neutrals are modeled as cold species. Wall energy losses and wall particle recombination are included in the model via equivalent frequencies. A sink is introduced in the energy equation to account for the ionization and radiation losses. Heat conduction is neglected in the model. The induced magnetic field is neglected and, consequently, the electric field derives from a potential ($\mathbf{E} = -\nabla\phi$). The resulting formulation may be written as [41]

$$\frac{d}{dx}(nv_{ex}) = \frac{d}{dx}(nv_{ix}) = -\frac{d}{dx}(n_n v_{nx}) = n(\nu_i - \nu_w) \tag{1}$$

$$m_i n_n v_{nx}\frac{dv_{nx}}{dx} = m_i n \nu_w (1-a_w)(v_{ix} - v_{nx}) \tag{2}$$

$$m_i n v_{ix}\frac{dv_{ix}}{dx} = -en\frac{d\phi}{dx} - m_i n \nu_i (v_{ix} - v_{nx}) \tag{3}$$

$$0 = -\frac{d}{dx}(nT_e) + en\frac{d\phi}{dx} - m_e n \nu_e \chi^2 v_{ex} \tag{4}$$

$$\frac{d}{dx}\left(\frac{5}{2}nT_e v_{ex}\right) = en v_{ex}\frac{d\phi}{dx} - n\nu_i E_i' - n\nu_{we}T_e \tag{5}$$

where x is the axial coordinate along the thruster channel; e, m_e, and m_i are the electron charge, electron mass, and ion mass, respectively; n_n and n are the neutral and plasma particle densities; v_{nx}, v_{ex}, and v_{ix} are the fluid axial velocities of neutrals, electrons, and ions, respectively; T_e and ϕ are the electron temperature and electric potential, respectively; ν_e is the effective electron collision frequency, $\nu_e = \nu_B + \nu_{wm} + \nu_{en}$, accounting for Bohm-type diffusion, ν_B, near-wall conductivity, ν_{wm}, and electron-neutral collisions, ν_{en}; ν_i, ν_w, and ν_{we} represent the frequencies for ionization, particle recombination, and energy losses at lateral walls, respectively; E_i' is the energy loss per actual created ion; and a_w is the accommodation factor of the ions impacting the walls [41]. The expression used for the Bohm-diffusion is $\nu_B = \alpha_B \omega_{ce}$, where ω_{ce} is the electron cyclotron frequency and α_B is a constant empirical coefficient whose value is typically selected so as to match experimental results ($\alpha_B \sim 0.01$). The electron momentum equation in the azimuthal direction, $v_{ey} = v_{ex}\chi$, where v_{ey} is the electron azimuthal velocity ($v_{ex} < 0, v_{ey} < 0$) and χ is the Hall parameter ($\chi = \omega_{ce}/\nu_e \gg 1$), has been used implicitly in the axial electron momentum equation. The combination of the previous equations allows obtaining an equation for the plasma density as

$$\frac{P}{n}\frac{dn}{dx} = G \tag{6}$$

where $P = T_e/m_i - (3/5)v_{ix}^2$, G is a function of the macroscopic variables, but not of their derivatives, and $P = 0$ is a sonic condition. It is possible to prove that there are two sonic points in the domain, one singular, $G \neq 0$, at the anode sheath transition, and another one regular, $G = 0$, inside the channel. A detailed description of the boundary conditions associated to the previous system of ordinary differential equations is described in [41]. Expressions for the different frequencies mentioned above (ν_{wm}, ν_{en}, ν_i, ν_e, ν_w, and ν_{we}) may also be found elsewhere [12], [41]–[43].

Various versions of the model presented above have been used in the past including different terms to characterize the Hall discharge [41], evaluate the influence of the

wall losses [12], carry out parametric investigations on the operating parameters [43], model two-stage Hall thrusters [44] and, even, analyze the stability of the discharge against axial perturbations to study the properties of the breathing mode [45]–[47].

B. General 2-D Formulation

A time-dependent 2-D model consistent with the equations presented in Section II-A is described here. The model considers two dimensions in space (axial, x, and azimuthal, y) and variations with time, t being the time variable. Under the same hypotheses of the 1-D model, the governing time-dependent 2-D equations of the plasma discharge may be written in nonconservative form as

$$\begin{aligned}\frac{\partial n}{\partial t}+\nabla\cdot(n\mathbf{v}_e) &= \frac{\partial n}{\partial t}+\nabla\cdot(n\mathbf{v}_i)\\ &= -\frac{\partial n_n}{\partial t}-\nabla\cdot(n_n\mathbf{v}_n)\\ &= n(\nu_i-\nu_w) \qquad (7)\end{aligned}$$

$$m_i n_n\left(\frac{\partial \mathbf{v}_n}{\partial t}+\mathbf{v}_n\cdot\nabla\mathbf{v}_n\right)=m_i n\nu_w(1-a_w)(\mathbf{v}_i-\mathbf{v}_n) \qquad (8)$$

$$m_i n\left(\frac{\partial \mathbf{v}_i}{\partial t}+\mathbf{v}_i\cdot\nabla\mathbf{v}_i\right)=-en\nabla\phi-m_i n\nu_i(\mathbf{v}_i-\mathbf{v}_n) \qquad (9)$$

$$\begin{aligned}0 &= -\nabla(nT_e)-en(-\nabla\phi+\mathbf{v}_e\times\mathbf{B})\\ &\quad -m_e n\nu_e\mathbf{v}_e \qquad (10)\end{aligned}$$

$$\frac{\partial}{\partial t}\left(\frac{3}{2}nT_e\right)+\nabla\cdot\left(\frac{5}{2}nT_e\mathbf{v}_e\right)=en\mathbf{v}_e\cdot\nabla\phi-n\nu_i E_i'-n\nu_{we}T_e \qquad (11)$$

where $\mathbf{v}_e$, $\mathbf{v}_i$, and $\mathbf{v}_n$ are the electron, ion, and neutral velocity vectors, respectively, and the rest of the symbols are as above.

In this 2-D case, the radial variation of the variables is neglected reducing the problem to two-dimensions. Moreover, curvature effects in the azimuthal direction are also neglected as the mean radius of the thruster is typically larger than the width of the channel. Obviously, in the limit of a stationary and axisymmetric solution, (7)–(11) reduce to (1)–(5).

Equations (7)–(11) can be rewritten in a form more adequate to this paper. To this end, the partial derivatives with respect to t and y, which will be Fourier transformed during the linearization, are moved to the right-hand side of the equations. In this manner, the left-hand side of the resulting equations resemble (1)–(5). Those resulting equations can be combined in order to obtain an equation for the plasma density as

$$\frac{P}{n}\frac{\partial n}{\partial x}=G+G_t+G_y \qquad (12)$$

where P and G are functions identical to the ones derived for the 1-D model and G_t and G_y are functions of the macroscopic variables and proportional to their time and azimuthal derivatives, respectively.

Apart from the sonic points mentioned above, it is important to note that the azimuthal component of (9) has the peculiarity of defining another special point along the channel. This equation may be expressed as

$$v_{ix}\frac{\partial v_{iy}}{\partial x}=-\nu_i(v_{iy}-v_{ny})-\frac{\partial v_{iy}}{\partial t}-\frac{e}{m_i}\frac{\partial\phi}{\partial y}-v_{iy}\frac{\partial v_{iy}}{\partial y} \qquad (13)$$

where v_{ny} and v_{iy} are the azimuthal neutral and ion velocities, respectively, and the rest of symbols are as above. This equation requires a regular transition at the point separating the ionization region and the ion back-streaming region ($v_{ix}=0$). Thus, the right-hand side of the equation must be zero at the same point as well. This fact has important consequences on the way the equations are solved numerically.

C. Linearization

Equations (7)–(11) can be linearized around the steady-state and axisymmetric solution (i.e., the zeroth-order background solution). To this end, it is possible to assume that any control parameter (say, w) of the Hall discharge (discharge voltage, mass flow, neutral velocity at the anode, and electron temperature at the cathode) may be written as the sum of a constant zeroth-order value, w_0, and a temporal-azimuthal perturbation, $\tilde{w}_1(y,t)$. If the perturbation is expressed as a Fourier expansion in y and t, then

$$w(y,t)=w_0+\Re\{w_1\exp(-i\omega t+ik_y y)\} \qquad (14)$$

where $\omega=\omega_r+i\omega_i$ is the angular frequency of the perturbation, being ω_r and ω_i its real and imaginary parts, and k_y is the azimuthal wave number of the perturbation. Note that k_y only admits a discrete number of values due to continuity conditions in the azimuthal direction, $k_y=-m/R$, where m is the integer mode number ($m>0$ when the perturbation travels in the $\mathbf{E}\times\mathbf{B}$ direction) and R is the mean radius of the thruster.

Similarly, a macroscopic variable, say $u(x,y,t)$, may be written as the sum of the axial zeroth-order solution, $u_0(x)$ and a perturbation, $\tilde{u}_1(x,y,t)$. The latter can also be Fourier expanded in t and y and, then, the complete solution may be expressed as

$$u(x,y,t)=u_0(x)+\Re\{u_1(x;\omega,k_y)\exp(-i\omega t+ik_y y)\}. \qquad (15)$$

The small perturbations hypothesis ($w_1\ll w_0$, $u_1\ll u_0$) allows linearizing (7)–(11) and decouple the evolution of the zero-th order solution, which is given in (1)–(5), from the evolution of the perturbations. Note that in order to consider consistently the axial gradients of the variables in this linearization, the zeroth-order solution and the coefficients of the Fourier expansion of the perturbations must retain the dependence on the axial coordinate. This is the main difference with respect to local stability analyses such as the one previously carried out in [48].

Applying (15) to (7)–(11), it is possible to obtain a linear system of equations with variable coefficients describing the evolution of the different perturbations along the channel. The resulting equations contain source terms proportional to the angular frequency, ω, and to the azimuthal wave number, k_y, of the perturbations. These equations must be solved several times, once for each fundamental mode associated to the boundary conditions. Moreover, the zeroth-order problem must also be solved together with the perturbation problem in order to be able to compute the coefficients of the perturbation equations.

The boundary conditions associated to the evolution equations of the Fourier coefficients of the perturbations are also derived linearizing the boundary conditions of the 1-D problem. This delicate linearization was detailed in [45].

D. Solution Method and Self-Excited Modes

The presence of a sonic point and a zero-ion-velocity point inside the thruster channel makes the integration process cumbersome. The solution is computed by concatenating the fundamental modes obtained integrating the equations from the anode and from those two internal points, whose location is unknown too. Obviously, the solution must be continuous in some intermediate points and this imposes more constraints to the final solution. Additional initial conditions are necessary to start the integration from the anode and those two internal points. In the end, the weights of the fundamental modes in the final solution are obtained from the following system of equations:

$$A\mathbf{x} = \mathbf{b} \tag{16}$$

where $\mathbf{x}$ is a vector containing the weights of the fundamental modes, $\mathbf{b}$ is a vector with the coefficients of the linearized control parameters and constraints, and A is a matrix with complex coefficients containing the partial derivatives of the control parameters with respect to the initial conditions of each of the fundamental modes. This matrix A depends on the vector of control parameters of the zeroth-order solution, $\mathbf{w}_0$, as well as on the angular frequency, ω, and on the wave number, k_y, of the perturbations, that is, $A = A(\mathbf{w}_0, \omega, k_y)$.

In order for self-excited modes to exist, the previous algebraic system of equations must have nontrivial solutions for the homogeneous problem (i.e., the case with $\mathbf{b} = \mathbf{0}$). This condition is equivalent to

$$\det A(\mathbf{w}_0, \omega, k_y) = 0 \tag{17}$$

where det is the determinant function.

For each zeroth-order solution given by the control parameters, $\mathbf{w}_0$, and each wave number, k_y, (17) provides a condition to compute the complex angular frequency, ω, of the perturbation. If the resulting angular frequency verifies the condition $\omega_i > 0$, then the perturbation is self-excited. In particular, the case $k_y = 0$ corresponds to purely axial oscillations studied in the past for the analysis of the breathing mode [45]–[47].

III. Results and Discussion

A. Reference Case and Background Solution

This section is devoted to the presentation of the results of the linearized time-dependent 2-D model for typical Hall thruster conditions. For this purpose, a SPT-100 thruster model has been considered as reference case. The main operating parameters of this case used in the simulation are presented in Table I, where the following symbols are used: $\dot{m}$ is the mass flow rate through the anode; V_d is the discharge voltage; $B_{\max}$ is the maximum magnetic field; $x_{\max}$ is the location of the maximum magnetic field with respect to the anode; $L_{\rm AE}$ is the distance from anode to external cathode; L_{ch}, h_c, and R are, respectively, the length, the width, and the mean radius of the channel; T_{eE} is the cathode temperature; v_{nB} is the neutral velocity at injection; α_B is the anomalous diffusion coefficient; $\tilde{\nu}_w$ is a dimensionless coefficient for the wall losses model [12]; and $T_{\rm SEE}$, which is also used in the wall losses model, is the electron temperature yielding 100% of secondary electron emission for the specific wall material. The electron temperature at the anode, T_{eB}, and the discharge current, I_d, are outputs of the simulation. For this reference case, these result in $T_{eB} = 1.2$ eV and $I_d = 5.0$A.

TABLE I

Main Operating Parameters of the SPT-100 Hall Thruster Used as Reference Case for the Simulations

$\dot{m}$	4.85 mg/s	V_d	300 V
B_{max}	237 G	x_{max}	20 mm
L_{ch}	25 mm	L_{AE}	33 mm
h_c	15 mm	R	42.5 mm
T_{eE}	4.8 eV	v_{nB}	300 m/s
α_B	0.01	$\tilde{\nu}_w$	0.16
T_{SEE}	100 V	a_w	1.0

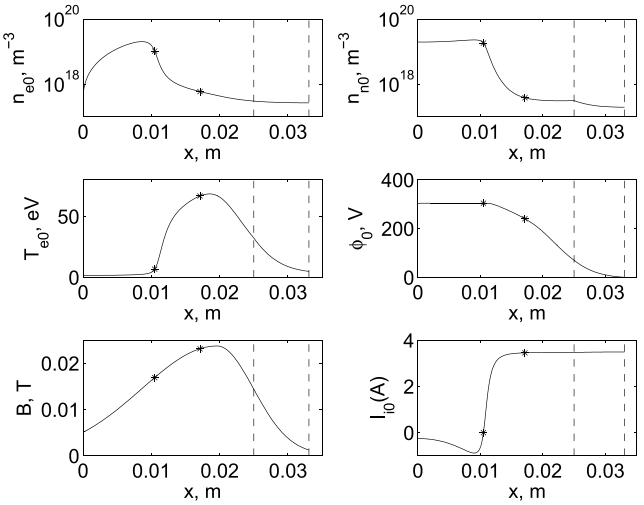

Fig. 1. Axial profiles of the main macroscopic variables of the background solution for the reference case. x is the axial location, $n_{e0}(x)$ is the plasma density, $n_{n0}(x)$ is the neutral density, $T_{e0}(x)$ is the electron temperature, $\phi_0(x)$ is the electric potential, $B(x)$ is the magnetic field, and $I_{i0}(x)$ is the ion axial current. The left asterisk corresponds to the zero-ion-velocity point, whereas the right asterisk corresponds to the regular sonic point inside the channel. The space between both points corresponds roughly to the ionization region of the thruster. The left vertical dashed line represents the channel exit, whereas the right one represents the location of the cathode, this is, the end of the simulation domain.

Fig. 1 shows the axial profiles of the main macroscopic variables corresponding to the background solution of (1)–(5) for the reference case described in Table I.

B. Azimuthal Oscillations

As a result of the global stability analysis of the reference case described in Table I, a self-excited oscillation is detected with an azimuthal mode number $m = 1$, a frequency $f = 11.1$ kHz, an azimuthal phase velocity $v_y = 2.6$ km/s, a growth-rate $\omega_i/2\pi \approx 3$ kHz, and an azimuthal wavelength

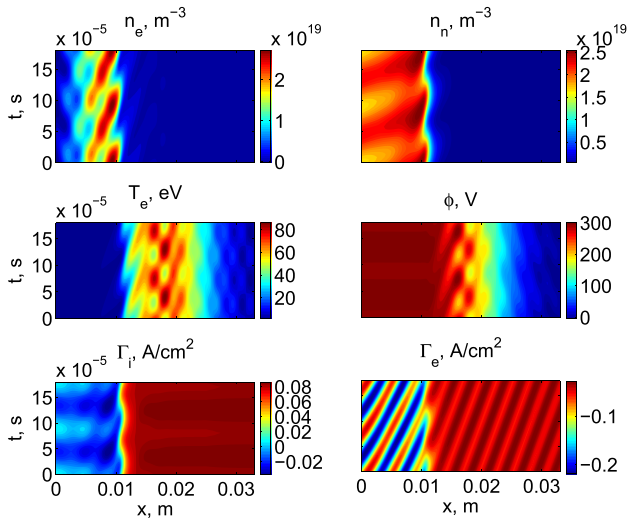

Fig. 2. Oscillations of the main macroscopic variables as combinations of the background solution and the perturbations shown as functions of x and t at $y = 0$ for a self-excited unstable oscillation of the perturbation problem for the reference case presented in Table I. The azimuthal mode number is $m = 1$, the frequency is $f = 11.1$ kHz, and the growth-rate is $\omega_i/2\pi \approx 3$ kHz. Variables represented (from left to right and top to bottom): plasma density, n_e; neutral density, n_n; electron temperature, T_e; electric potential, ϕ; ion axial flux, Γ_i; electron axial flux, Γ_e. Perturbations artificially set to 30% of the base solution.

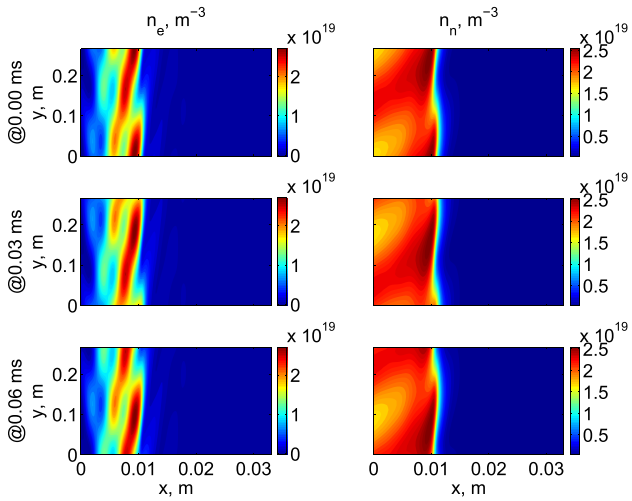

Fig. 3. Oscillations of the main macroscopic variables as combinations of the background solution and the perturbations shown as functions of x and y at different values of t (at t millisecond) for the same conditions used previously in Fig. 2. Variables represented (from left to right): plasma density, n_e and neutral density, n_n. Perturbations artificially set to 30% of the base solution.

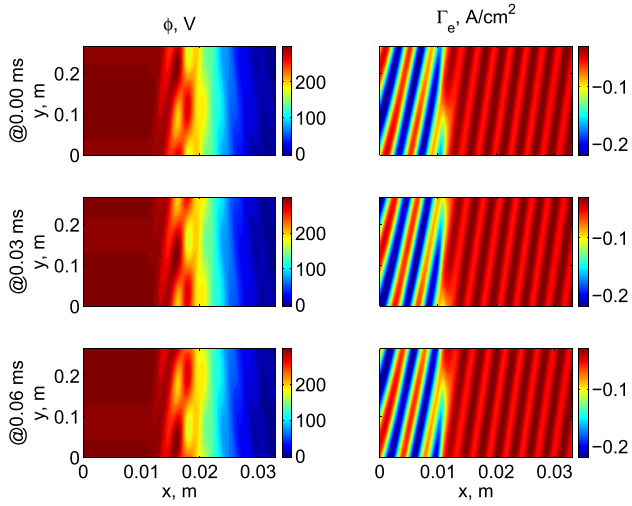

Fig. 4. Same as Fig. 3 for other macroscopic variables. Variables represented (from left to right): electric potential, ϕ and electron axial flux, Γ_e.

$k_y = -0.023$ mm^{-1}. According to these values, the simulated azimuthal oscillation has properties similar to those experimentally observed for the spoke. As it will be shown later, its growth rate is similar to the corresponding one for the breathing mode ($m = 0$). Thus, it is not clear from this analysis which oscillation, the azimuthal one or the axial one, dominates in the reference case.

It must be noted that other mode numbers ($m = -2$, -1, and 2) have been analyzed looking for possible self-excited solutions. However, for the reference case under consideration the only mode numbers resulting in self-excited solutions are $m = 0$ (breathing mode) and $m = 1$ (spoke). This is in line with experimental results for normal-size thrusters, where the spoke is normally detected as a single oscillation in the $\mathbf{E} \times \mathbf{B}$ direction. In the case of larger thrusters, experiments show that higher modes ($m = 2, 3, 4$) might become dominant [25]. The scaling of the azimuthal oscillations simulated here to bigger thrusters has not been investigated yet.

Fig. 2 shows the contour maps in the $x - t$ space (at the meridian section $y = 0$) of the main macroscopic variables as combinations of the background solution and the perturbations for the self-excited oscillation mentioned above. As the size of the perturbations does not result from the linear perturbations problem, it must be chosen arbitrarily. Just for illustration purposes, this size has been selected so that $T_{e1}/T_{e0} = 30\%$ at the location of the peak of the profile of the temperature perturbation, and the exponential dependence $\exp(-i\omega_i t)$ has been omitted. This choice does not impact the results presented in this section, where the focus is on the stable/unstable character of the linear oscillations and on the physical mechanism behind them. The selected size is justified as nonetheless typical saturated spoke oscillations have a size of similar magnitude as the background state. In any case, it is true that the saturation of the oscillation may occur and the real shape of the saturated spoke oscillation may be different from the one represented here.

Figs. 3 and 4 show contour maps in the x–y space for different instants of time, t, during one cycle of the azimuthal oscillation under the same conditions as in Fig. 2. In this figure, it is possible to observe how the oscillation travels in the y-direction, this is, in the $+\,\mathbf{E} \times \mathbf{B}$ direction. As expected, the same patterns shown in Fig. 2 are observed in Figs. 3 and 4 moving in the azimuthal direction.

According to Figs. 3 and 4, the azimuthal oscillation is due to an azimuthal variation of the ionization process. The connection between the spoke oscillation and the ionization process had already been suggested theoretically in [35] and [48], and, based on experiments, by other researchers [49]. This fact is further analyzed in Section III-C,

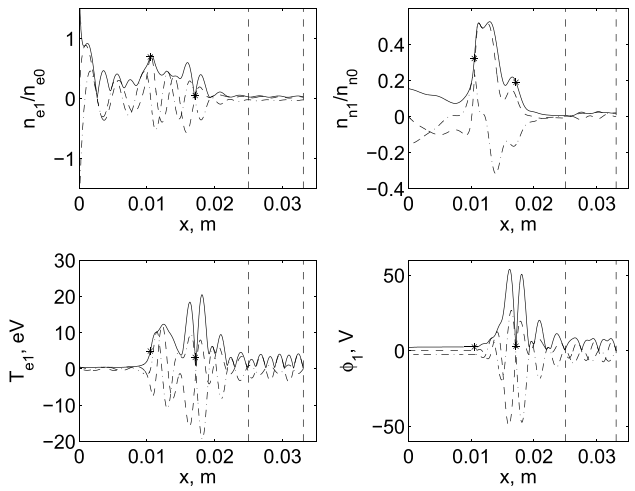

Fig. 5. Axial profiles of the coefficients of the Fourier-expanded perturbations of the main macroscopic variables corresponding to the self-excited unstable oscillation of the perturbation problem for the reference case presented in Table I and the same conditions as in Fig. 2. Variables represented: x is the axial location, n_{e1}/n_{e0} is the perturbation of the plasma density over the background plasma density, n_{n1}/n_{n0} is the perturbation of the neutral density over the background neutral density, T_{e1} is the perturbation of the electron temperature, ϕ_1 is the perturbation of the electric potential. Dashed lines are used for the real part of the perturbation coefficients, dashed-dotted lines are used for the imaginary part and continuous lines are used for the modulus of the perturbation coefficients. In each plot, the left dashed vertical line represents the channel exit and the right one the end of the simulation domain. Perturbations artificially set to 30% of the base solution.

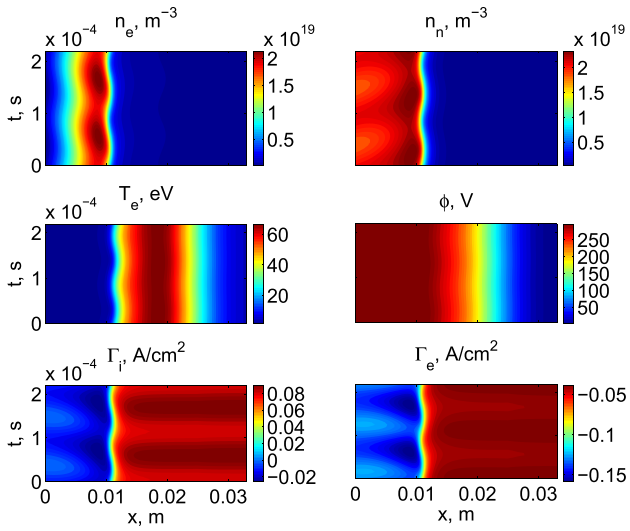

Fig. 6. Oscillations as a function of x and t for the breathing mode ($m = 0$). The conditions and variables are similar to those shown in Fig. 2.

where the azimuthal oscillation is compared with the breathing mode.

From Figs. 2–4, it is possible to compute the approximate wavelength of the oscillation in the axial direction, k_x. This is estimated to be $k_x \approx 1.7$ mm^{-1}, which is consistent with a wave travelling forward in the axial direction ($\omega_r > 0$, $k_x > 0$) at a fixed azimuth and in the $+\ \mathbf{E} \times \mathbf{B}$ direction ($\omega_r > 0$, $k_y < 0$) at a fixed axial location as time increases.

However, the tilt angle with respect to the axis of the thruster ($\tan\beta = k_x/k_y$) is close to 90°, whereas in experiments, the azimuthal oscillation is normally observed to have a tilt angle around 15°–20° [10], [19]. The reason for this discrepancy is believed to be related to the narrow ionization region seen in the simulation, likely caused by the fact that heat conduction effects are not considered in the model. The version of the 1-D model of Ahedo *et al.* [42] that takes into consideration heat conduction terms gives smoother temperature profiles, wider ionization regions, and lower temperatures inside the thruster. Thus, adding heat conduction effects to the model might reduce the tilt angle of the azimuthal oscillation considerably.

For completeness, Fig. 5 shows the axial profiles of the complex coefficients of the Fourier expansion of the perturbation equations defined in (15). These are the variables resulting from the integration of the linearized equations.

Based on Fig. 5, it is also interesting to point out that the perturbed electric field has a roughly constant azimuthal component upstream of the ionization region (see left column of Fig. 4 and plot of ϕ_1 in Fig. 5). This fact, together with the plasma density variation, causes an oscillatory axial electron current to the anode coming from the $\mathbf{E} \times \mathbf{B}$ drift associated to the azimuthal electric field, as can be observed in the right column of Fig. 4.

C. Comparison With the Breathing Mode

Similar to Fig. 2, Fig. 6 shows the contour maps in the x–t space of the main variables for an unstable oscillation with $m = 0$ for the very same reference case presented in Table I. The frequency of the unstable oscillation is $f = 9.1$ kHz, whereas the growth-rate is $\omega_i/2\pi \approx 3$ kHz, similar to the spoke by chance. The frequency of the simulated breathing mode is smaller than for the azimuthal oscillation presented previously, as normally observed in experiments [15], [19].

In the azimuthal oscillation (see plot of neutral density in Fig. 2), the ionization front moves back and forth, as in the breathing mode (Fig. 6). Moreover, the $m = 1$ oscillation also shows a travelling wave of neutral density, as in the breathing mode. The similarity with the breathing mode, thus, seems clear. The fact that both modes are recovered with the very same model reinforces this idea. Moreover, as in the case of the $m = 1$ oscillation, the region where the ionization front moves back and forth is rather thin compared to what is normally seen experiments for the breathing mode.

Similarly, Smith and Cappelli [21] present experimental results, giving evidence of a complex helical oscillation in plasma potential, which seems to be caused by an interaction between the breathing mode and the spoke oscillations. This gives additional support to the idea of a similar mechanism for the breathing mode and the azimuthal spoke. Note, however, that the oscillation from [21] is observed in the thruster plume rotating in the opposite direction to what is observed in this paper.

Another interesting property common to both oscillations is the nonuniformity, in space and time, of the neutral density at the anode plane. This seems in contradiction with the imposed anode boundary conditions that enforce uniform neutral velocity and mass flow rate. The reason for the neutral density to be nonuniform at the anode resides in the neutral

recombination at the back wall of the thruster. Indeed this may be one of the reasons why the breathing mode and the spoke oscillation are unstable as it is explained next. Part of the ions generated in the ionization region are attracted to the anode through the ion-backstreaming region and are recombined into neutrals. These neutrals travel downstream and are available for subsequent ionization cycles and, thus, more ions than in previous ionization cycles are generated and sent back to the anode. The complete process is repeated again and, hence, the growing character of this mechanism.

IV. Anomalous Diffusion and Azimuthal Oscillations

The formulation presented above has mostly focused on the analysis of the linear stability of the Hall discharge against azimuthal perturbations. In case a self-excited oscillation is detected, then unstable oscillations grow and eventually saturate. The linear growth phase is the only one modeled with the 2-D model presented here, whereas the saturation is a nonlinear process. Anomalous diffusion related to saturated azimuthal oscillations cannot be determined self-consistently here. Nonetheless, some insight can be obtained if we accept the following postulate. The shape and relative strength of the saturated oscillations are those corresponding to the linear perturbations solution. Of course the postulate is less true the higher is the strength of the saturated oscillation, a parameter totally outside of the scope of the linear model used here.

Equation (10) is indeed the Ohm's law for electrons and can be expressed as

$$en_e\mathbf{v}_e = -\boldsymbol{\mu}(en_e\mathbf{E} + \nabla(n_eT_e)) \tag{18}$$

where $\boldsymbol{\mu}$ is the electron mobility tensor and the rest of symbols as above. In the directions x and y, we have

$$en_e v_{ex} = -\mu_\perp\left(en_eE_x + \frac{\partial n_eT_e}{\partial x}\right) + \mu_H\left(en_eE_y + \frac{\partial n_eT_e}{\partial y}\right) \tag{19}$$

$$en_e v_{ey} = -\mu_\perp\left(en_eE_y + \frac{\partial n_eT_e}{\partial y}\right) - \mu_H\left(en_eE_x + \frac{\partial n_eT_e}{\partial x}\right) \tag{20}$$

where the components of the mobility tensor are defined as

$$\mu_\perp = \frac{e}{m_e}\frac{\nu_e}{\omega_{ce}^2+\nu_e^2} \simeq \frac{1}{B\chi} \tag{21}$$

$$\mu_H = \chi\mu_\perp \simeq \frac{1}{B}. \tag{22}$$

For an axisymmetric solution, the last term of (19) and (20) is zero. However, if small azimuthal oscillations are present, and because of $\mu_H \gg \mu_\perp$, the last term in (19) may be important, thus providing an extra contribution to axial (i.e., perpendicular) transport. The azimuthal oscillations are not expected to modify significantly the rest of equations.

Next, the effect of that oscillation-based transport on the 1-D steady-state solution will come out from averaging its effect over t and y. This yields

$$en_{e0}v_{ex0} = -\mu_{\perp 0}\left(en_eE_x + \frac{\partial n_eT_e}{\partial x}\right)_0 + \frac{\langle en_{e1}E_{y1}\rangle}{B} \tag{23}$$

$$en_{e0}v_{ey0} \simeq -\mu_H\left(en_eE_x + \frac{\partial n_eT_e}{\partial x}\right)_0 \tag{24}$$

where $\langle z\rangle(x)$ is the temporal-azimuthal average of a function $z(t,x,y)$.

The strength of the oscillation-based transport, measured as the azimuthal force relative to the axial one, is expressed as

$$\alpha_A(x) = \frac{\langle n_1E_{y1}\rangle}{n_0v_{ey0}B} \tag{25}$$

so that we can rearrange (23) and (24) as

$$v_{ey0} = \frac{\omega_{ce}}{\nu_e'}v_{ex0} \tag{26}$$

$$\text{with} \quad \nu_e' = \nu_e + \alpha_A(x)\omega_{ce}. \tag{27}$$

The last expression for ν_e' resembles the definition of the Bohm-diffusion frequency ($\nu_B = \alpha_B\omega_{ce}$) highlighting the relation between the anomalous transport and the oscillation-based transport. If this additional transport were all the anomalous contribution, then $\alpha_B = \alpha_A(x)$, however, there may be other contributors to the anomalous diffusion. From a practical point of view, given the perturbations of plasma density and azimuthal electric field, (25) allows obtaining the equivalent anomalous diffusion coefficient associated to the perturbations.

Note in any case that term is a nonlinear effect and thus it is not accounted for in the formulation used in the previous sections, where the zeroth- and first-order problems are solved. In order to close the loop and have a self-consistent linear model of the oscillation-based transport it would be necessary to impose $\alpha_B = \alpha_A(x)$ and iterate until the same profile used in the zeroth-order solution results from the corresponding linear perturbation problem.

One of the consequences of the azimuthal oscillation may thus be enhanced electron conductivity inside the channel. In order to evaluate the net effect on the electron current, it is convenient to compute the equivalent anomalous diffusion coefficient, $\alpha_A(x)$, associated to the perturbations computed with the linear model. Fig. 7 shows the axial variation of $\alpha_A(x)$ based on (25). It is possible to observe that the net effect of the oscillation on the electron conductivity is concentrated

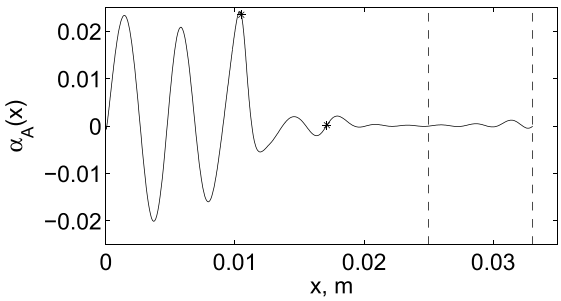

Fig. 7. Axial profiles of the equivalent anomalous diffusion coefficient, $\alpha_A(x)$, as computed from the linear perturbation with a size of 30% of the zeroth-order solution. Symbols are as in Fig. 4.

in the rear part of the thruster, more precisely, in the ion-backstreaming region. The values reached by $\alpha_A(x)$ in this region are of the same order of magnitude to that used for α_B in the simulation of the background solution of the reference case (Table I). In fact, for the case under analysis the average value of $\alpha_A(x)$ in the rear part of the thruster is $\alpha_{A,\text{ave}} \approx 0.01$, a value very similar to the one used in the zeroth-order solution. However, this is only true for the selected size of linear oscillations that, as mentioned above, is such that the maximum temperature perturbation is 30% of the background temperature.

Another relevant aspect is the fact that $\alpha_A(x)$ reaches negative values in some regions of the channel. This negative value of $\alpha_A(x)$ is linked to the tilt angle close to 90° of the plasma density perturbation, which causes a change of phase between the perturbations of the plasma density and the azimuthal electric field. Moreover, the large variations of $\alpha_A(x)$ anticipate important changes in the background solution, where so far α_B has been considered constant, in case the profile of $\alpha_A(x)$ is used in the resolution of the zeroth-order problem. Anyway, no contribution to electron conductivity is seen downstream of the ionization region, where experiments also show a higher than expected electron mobility. Nonlinear effects affecting the low-frequency azimuthal oscillation might resolve this contradiction. Another possible explanation is that high-frequency oscillations (1–10 MHz) [50]–[54] might play a role in that region.

V. Conclusion

A linearized time-dependent 2-D model has been used for the analysis of the global azimuthal stability of the Hall discharge. Contrary to more common local analyses, this approach takes into account consistently the axial variation of the plasma variables. Results show an unstable self-excited azimuthal oscillation travelling in the $+\,\mathbf{E}\times\mathbf{B}$ direction with a mode number $m = 1$, a phase velocity $v_y = 2.6$ km/s and a frequency around 11 kHz. These features are similar to those experimentally observed for the so-called spoke. The analysis of the oscillation and the comparison with the breathing mode reveal that the ionization might be a driver for the azimuthal variation of the plasma and neutral densities. Moreover, first estimates of the electron conductivity caused by the azimuthal linear oscillation show a non-negligible contribution in the rear part of the thruster, but not in the acceleration region. It is important to note that even though the unstable/stable character of the small azimuthal oscillations presented here is not altered by the linear hypothesis on which the study is based, the latter conclusion about the modified electron conductivity is indeed affected.

As part of future work, the main activity to be carried out is the understanding of the mechanism of the azimuthal oscillation and the scaling with the thruster size and the different operating parameters. Beyond this, we identify the following areas of research. First, a comparison between the stability criteria derived from the local stability analyses of [29]–[31] and [35] and the results from the global stability presented here seems very appealing. This can be achieved by analyzing the local stability of the axial profiles of the reference case and comparing the results against the global ones presented here. This should allow us to identify the local stability analysis that best matches the global one, if any. Second, we intend to extend the linearized time-dependent 2-D model to high frequency (1–10 MHz) so that electron drift oscillations [50]–[53] in the azimuthal direction can be analyzed numerically. This paper would continue the theoretical work already carried out in previous studies [36], [39]. Finally, the introduction of heat conduction effects should be considered to analyze its impact on the azimuthal oscillation simulated here. A further step on the analysis of the spoke would consist in considering nonlinear effects in order to model properly the saturation of the oscillations and reproduce consistently real-size spokes.

References

[1] A. I. Morozov, Y. Esipchuk, G. N. Tilinin, A. V. Trofimov, Y. A. Sharov, and G. Y. Shchepkin, "Plasma accelerator with closed electron drift and extended acceleration zone," *Soviet Phys.-Tech. Phys.*, vol. 17, no. 1, pp. 38–45, 1972.

[2] N. B. Meezan and M. A. Cappelli, "Electron density measurements for determining the anomalous electron mobility in a coaxial Hall discharge plasma," in *Proc. 36th Joint Propuls. Conf. Exhibit*, 2000, Art. ID. AIAA-2000-3420.

[3] J. A. Linnell and A. D. Gallimore, "Hall thruster electron motion characterization based on internal probe measurements," in *Proc. 31st Int. Electr. Propuls. Conf.*, 2009, Art. ID. IEPC-2009-105. [Online]. Available: http://www.erps.spacegrant.org

[4] N. B. Meezan, W. A. Hargus, Jr., and M. A. Cappelli, "Anomalous electron mobility in a coaxial Hall discharge plasma," *Phys. Rev. E*, vol. 63, no. 2, p. 026410, Jan. 2001.

[5] M. A. Cappelli, N. B. Meezan, and N. Gascon, "Transport physics in Hall plasma thrusters," in *Proc. 40th AIAA Aerosp. Sci. Meeting Exhibit*, 2002, Art. ID AIAA-2002-0485.

[6] C. Boniface, L. Garrigues, G. J. M. Hagelaar, J. P. Boeuf, D. Gawron, and S. Mazouffre, "Anomalous cross field electron transport in a Hall effect thruster," *Appl. Phys. Lett.*, vol. 89, no. 16, p. 161503, 2006.

[7] D. Gawron, S. Mazouffre, and C. Boniface, "A Fabry–Pérot spectroscopy study on ion flow features in a Hall effect thruster," *Plasma Sour. Sci. Technol.*, vol. 15, no. 4, pp. 757–764, 2006.

[8] A. I. Morozov, Y. V. Esipchuk, A. M. Kapulkin, V. A. Nevrovskii, and V. A. Smirnov, "Effect of the magnetic field on a closed-electron-drift accelerator," *Soviet Phys.-Tech. Phys.*, vol. 17, no. 3, pp. 482–487, 1972.

[9] S. Yoshikawa and D. J. Rose, "Anomalous diffusion of a plasma across a magnetic field," *Phys. Fluids*, vol. 5, no. 3, p. 334, 1962.

[10] G. S. Janes and R. S. Lowder, "Anomalous electron diffusion and ion acceleration in a low-density plasma," *Phys. Fluids*, vol. 9, no. 6, p. 1115, 1966.

[11] A. I. Morozov, "Conditions for efficient current transport by near-wall conduction," *Soviet Phys. Tech. Phys.*, vol. 32, no. 8, pp. 901–904, 1987.

[12] E. Ahedo, J. M. Gallardo, and M. Martińez-Sánchez, "Effects of the radial plasma-wall interaction on the Hall thruster discharge," *Phys. Plasmas*, vol. 10, no. 8, p. 3397, 2003.

[13] L. Garrigues, G. J. M. Hagelaar, C. Boniface, and J. P. Boeuf, "Anomalous conductivity and secondary electron emission in Hall effect thrusters," *J. Appl. Phys.*, vol. 100, no. 12, p. 123301, 2006.

[14] F. I. Parra, E. Ahedo, J. M. Fife, and M. Martínez-Sánchez, "A two-dimensional hybrid model of the Hall thruster discharge," *J. Appl. Phys.*, vol. 100, no. 2, p. 023304, 2006.

[15] E. Y. Choueiri, "Plasma oscillations in Hall thrusters," *Phys. Plasmas*, vol. 8, no. 4, p. 1411, 2001.

[16] Y. B. Esipchuk, A. I. Morozov, G. N. Tilinin, and A. V. Trofimov, "Plasma oscillations in closed-drift accelerators with an extended acceleration zone," *Soviet Phys. Tech. Phys.*, vol. 18, no. 7, pp. 928–932, 1974.

[17] P. J. Lomas and J. D. Kilkenny, "Electrothermal instabilities in a Hall accelerator," *Plasma Phys.*, vol. 19, no. 4, p. 329, 1977.

[18] W. A. Hargus, N. B. Meezan, and M. A. Cappelli, "A study of a low power Hall thruster transient behavior," in *Proc. 25th Int. Electr. Propuls. Conf.*, 1997, pp. 351–358.

[19] E. Chesta, C. M. Lam, N. B. Meezan, D. P. Schmidt, and M. A. Cappelli, "A characterization of plasma fluctuations within a Hall discharge," *IEEE Trans. Plasma Sci.*, vol. 29, no. 4, pp. 582–591, Aug. 2001.

[20] N. Gascon and M. Cappelli, "Plasma instabilities in the ionization regime of a Hall thruster," in *Proc. 29th Joint Propuls. Conf.*, 2003, Art. ID AIAA-2003-4857.

[21] A. W. Smith and M. A. Cappelli, "Time and space-correlated plasma potential measurements in the near field of a coaxial Hall plasma discharge," *Phys. Plasmas*, vol. 16, no. 7, p. 073504, 2009.

[22] Y. Raitses, A. Smirnov, and N. J. Fisch, "Effects of enhanced cathode electron emission on Hall thruster operation," *Phys. Plasmas*, vol. 16, no. 5, p. 057106, 2009.

[23] J. B. Parker, Y. Raitses, and N. J. Fisch, "Transition in electron transport in a cylindrical Hall thruster," *Appl. Phys. Lett.*, vol. 97, no. 9, pp. 091501-1–091501-3, Aug. 2010.

[24] C. L. Ellison, Y. Raitses, and N. J. Fisch, "Fast camera imaging of Hall thruster ignition," *IEEE Trans. Plasma Sci.*, vol. 39, no. 11, pp. 2950–2951, Nov. 2011.

[25] M. S. McDonald and A. D. Gallimore, "Parametric investigation of the rotating spoke instability in Hall thrusters," in *Proc. 32nd Int. Electr. Propuls. Conf.*, 2011, Art. ID IEPC-2011-242. [Online]. Available: http://www.erps.spacegrant.org

[26] D. Liu, *Two-Dimensional Time-Dependent Plasma Structures of a Hall-Effect Thruster*, Ph.D. dissertation, Graduate School Eng. Manage., Air Force Inst. Technol., Wright-Patterson AFB, OH, USA, 2011.

[27] Y. V. Esipchuk and G. N. Tilinin, "Drift instability in a Hall-current plasma accelerator," *Soviet Phys.-Tech. Phys.*, vol. 21, no. 4, pp. 417–423, 1976.

[28] A. Kapulkin and M. Guelman, "Low frequency instability and enhanced transfer of electrons in near-anode region of Hall thruster," in *Proc. 30th Int. Electr. Propuls. Conf.*, 2007, Art. ID IEPC-2007-079. [Online]. Available: http://www.erps.spacegrant.org

[29] A. Kapulkin and M. M. Guelman, "Low-frequency instability in near-anode region of Hall thruster," *IEEE Trans. Plasma Sci.*, vol. 36, no. 5, pp. 2082–2087, Oct. 2008.

[30] W. Frias, A. I. Smolyakov, I. D. Kaganovich, and Y. Raitses, "Long wavelength gradient drift instability in Hall plasma devices. I. Fluid theory," *Phys. Plasmas*, vol. 19, no. 7, p. 072112, 2012.

[31] A. I. Smolyakov, W. Frias, Y. Raitses, and N. J. Fisch, "Gradient instabilities in Hall thruster plasmas," in *Proc. 32nd Int. Electr. Propuls. Conf.*, 2011, Art. ID IEPC-2011-271.

[32] E. Chesta, N. B. Meezan, and M. A. Cappelli, "Stability of a magnetized Hall plasma discharge," *J. Appl. Phys.*, vol. 89, no. 6, pp. 3099–3107, Mar. 2001.

[33] J. Gallardo and E. Ahedo, "On the anomalous diffusion mechanism in Hall-effect thrusters," in *Proc. 29th Int. Electr. Propuls. Conf.*, 2005, Art. ID. IEPC-2005-117.

[34] H. K. Malik and S. Singh, "Resistive instability in a Hall plasma discharge under ionization effect," *Phys. Plasmas*, vol. 20, no. 5, p. 052115, 2013.

[35] D. Escobar and E. Ahedo, "Low frequency azimuthal stability of the ionization region of the Hall thruster discharge. I. Local analysis," *Phys. Plasmas*, vol. 21, no. 4, p. 043505, 2014.

[36] A. A. Litvak and N. J. Fisch, "Rayleigh instability in Hall thrusters," *Phys. Plasmas*, vol. 11, no. 4, p. 1379, 2004.

[37] A. M. Kapulkin and V. F. Prisnyakov, "Dissipative method of suppression of electron drift instability in SPT," in *Proc. 24th Int. Electr. Propuls. Conf.*, 1995, pp. 302–306, Art. ID IEPC-95-37.

[38] A. Kapulkin, J. Ashkenazy, A. Kogan, G. Appelbaum, D. Alkalay, and M. Guelman, "Electron instabilities in Hall thrusters: Modelling and application to electric field diagnostics," in *Proc. 28th Int. Electr. Propuls. Conf.*, 2003, Art. ID IEPC-2003-100.

[39] A. Kapulkin and M. Guelman, "Lower-hybrid instability in Hall thruster," in *Proc. 29th Int. Electr. Propuls. Conf.*, 2005, Art. ID IEPC-2005-088. [Online]. Available: http://www.erps.spacegrant.org

[40] H. K. Malik and S. Singh, "Conditions and growth rate of Rayleigh instability in a Hall thruster under the effect of ion temperature," *Phys. Rev. E*, vol. 83, no. 3, p. 036406, 2011.

[41] E. Ahedo, P. Martińez-Cerezo, and M. Martińez-Sánchez, "One-dimensional model of the plasma flow in a Hall thruster," *Phys. Plasmas*, vol. 8, no. 6, p. 3058, 2001.

[42] E. Ahedo, J. M. Gallardo, and M. Martińez-Sánchez, "Model of the plasma discharge in a Hall thruster with heat conduction," *Phys. Plasmas*, vol. 9, no. 9, p. 4061, 2002.

[43] E. Ahedo and D. Escobar, "Influence of design and operation parameters on Hall thruster performances," *J. Appl. Phys.*, vol. 96, no. 2, p. 983, 2004.

[44] E. Ahedo and F. I. Parra, "A model of the two-stage Hall thruster discharge," *J. Appl. Phys.*, vol. 98, no. 2, pp. 023303-1–023303-11, Jul. 2005.

[45] E. Ahedo, P. Martínez, and M. Martínez-Sánchez, "Steady and linearly-unsteady analysis of a Hall thruster with an internal sonic point," in *Proc. 36th AIAA/ASME/SAE/ASEE Joint Propuls. Conf. Exhibit*, 2000, Art. ID AIAA-2000-3655.

[46] R. Noguchi, M. Martínez-Sánchez, and E. Ahedo, "Linear 1-D analysis of oscillations in Hall thrusters," in *Proc. 26th Int. Electr. Propuls. Conf.*, 1999, Art. ID IEPC-99-105. [Online]. Available: http://www.erps.spacegrant.org

[47] S. Barral, V. Lapuerta, A. Sanch, and E. Ahedo, "Numerical investigation of low-frequency longitudinal oscillations in Hall thrusters," in *Proc. 29th Int. Electr. Propuls. Conf.*, 2005, Art. ID IEPC-2005-120. [Online]. Available: http://www.erps.spacegrant.org

[48] D. Escobar and E. Ahedo, "Ionization-induced azimuthal oscillation in Hall effect thrusters," in *Proc. 32nd Int. Electr. Propuls. Conf.*, 2011, Art. ID IEPC-2011-196.

[49] A. Vesselovzorov, E. Dlougach, E. Pogorelov, A. A. Svirskiy, and V. Smirnov, "Low-frequency wave experimental investigations, transport and heating of electrons in stationary plasma thruster SPT," in *Proc. 32nd Int. Electr. Propuls. Conf.*, 2011, Art. ID IEPC-2011-060. [Online]. Available: http://www.erps.spacegrant.org

[50] G. Guerrini and C. Michaut, "Characterization of high frequency oscillations in a small Hall-type thruster," *Phys. Plasmas*, vol. 6, no. 1, p. 343, 1999.

[51] A. A. Litvak, Y. Raitses, and N. J. Fisch, "Experimental studies of high-frequency azimuthal waves in Hall thrusters," *Phys. Plasmas*, vol. 11, no. 4, p. 1701, 2004.

[52] A. Lazurenko, V. Krasnoselskikh, and A. Bouchoule, "Experimental insights into high-frequency instabilities and related anomalous electron transport in Hall thrusters," *IEEE Trans. Plasma Sci.*, vol. 36, no. 5, pp. 1977–1988, Oct. 2008.

[53] A. K. Knoll and M. A. Cappelli, "Experimental characterization of high frequency instabilities within the discharge channel of a Hall thruster," in *Proc. 31st Int. Electr. Propuls. Conf.*, 2009, Art. ID IEPC-2009-099. [Online]. Available: http://www.erps.spacegrant.org

[54] S. Tsikata, C. Honore, D. Gresillon, A. Heron, N. Lemoine, and J. Cavalier, "The small-scale high-frequency E×B instability and its links to observed features of the Hall thruster discharge," in *Proc. 33rd Int. Electr. Propuls. Conf.*, 2013, Art. ID IEPC-2013-261. [Online]. Available: http://www.erps.spacegrant.org

Diego Escobar received the M.Sc. and M.A.S. degrees in aeronautical engineering from the Universidad Politécnica de Madrid, Madrid, Spain, in 2005 and 2007, respectively. He is currently pursuing the Ph.D. degree from the Universidad Politécnica de Madrid, Madrid, Spain.

He was an Aerospace Engineer with the European Space Operations Centre, Darmstadt, Germany, from 2007 to 2011. He is currently the Project Manager with GMV, Madrid. His current research interests include modeling and simulation in Hall thrusters and satellite orbital dynamics and navigation in the professional field.

Eduardo Ahedo received the M.Sc. and Ph.D. degrees in aeronautical engineering from the Universidad Politécnica de Madrid, Madrid, Spain, in 1982 and 1988, respectively.

He was a Fullbright Post-Doctoral Scholar with the Massachusetts Institute of Technology, Cambridge, MA, USA, from 1989 to 1990. He is currently a Professor of Aerospace Engineering with the Universidad Carlos III de Madrid, Leganés, Spain. His current research interests include modeling and simulation in plasma propulsion, electrodynamic tethers, plasma contactors, plasma-surface interactions, plasma instabilities, and plasma-laser interactions.